An ensemble Kalman filter for the time-dependent analysis of the geomagnetic field

Alexandre Fournier, Lars Nerger, Julien Aubert

Geochemistry Geophysics Geosystems G3

Technical Brief
Volume 14, Number 10
2 October 2013
doi: 10.1002/ggge.20252
ISSN: 1525-2027

Published by AGU and the Geochemical Society

An ensemble Kalman filter for the time-dependent analysis of the geomagnetic field

Alexandre Fournier
Géomagnétisme, Institut de Physique du Globe de Paris, Sorbonne Paris Cité, Université Paris Diderot, UMR 7154 CNRS, F-75005, Paris, France (fournier@ipgp.fr)

Lars Nerger
Alfred Wegener Institute, Helmholtz Center for Polar and Marine Research, Am Handelshafen 12, D-27570, Bremerhaven, Germany

Julien Aubert
Dynamique des fluides géologiques, Institut de Physique du Globe de Paris, Sorbonne Paris Cité, Université Paris Diderot, UMR 7154 CNRS, F-75005, Paris, France

[1] We present the application of the ensemble Kalman filter to a three-dimensional, convection-driven model of the geodynamo. Our implementation rests on a suitably modified version of the parallel data assimilation framework of Nerger and Hiller (2013). We resort to closed-loop experiments for validation purposes, using a dynamo model of intermediate resolution. Observations for these experiments consist of spectral coefficients describing the surface poloidal magnetic field, with arbitrary truncation. Our synthetic tests demonstrate the efficacy and adaptivity of the method, provided the ensemble comprises $\mathcal{O}(500)$ members, in which case the typical spin-up time we find for our system is $\mathcal{O}(1000)$years. In case of a poor resolution of the observations, we find that the knowledge of the full covariance matrix describing the uncertainty affecting the spectral coefficients (as opposed to its sole diagonal) results in a much better estimate of the internal structure of the dynamo.

Components: 9,113 words, 3 figures, 1 table.

Keywords: geomagnetism; data assimilation; numerical dynamo models.

Index Terms: 1910 Data assimilation, integration and fusion: Informatics; 1932 High-performance computing: Informatics; 1510 Dynamo: theories and simulations: Geomagnetism and Paleomagnetism; 1560 Time variations: secular and longer: Geomagnetism and Paleomagnetism; 3260 Inverse theory: Mathematical Geophysics.

Received 5 July 2013; **Revised** 14 August 2013; **Accepted** 14 August 2013; **Published** 2 October 2013.

Fournier, A., L. Nerger, and J. Aubert. (2013), An ensemble Kalman filter for the time-dependent analysis of the geomagnetic field. *Geochem. Geophys. Geosyst.*, *14*, 4035–4043, doi:10.1002/ggge.20252.

1. Introduction

[2] The past few years have seen a surge of activity related to the potential application of data assimilation techniques to the analysis of the geomagnetic field [e.g., *Fournier et al.*, 2010; *Kuang and Tangborn*, 2011, for reviews]. Data assimilation aims at combining in an optimal fashion the information contained in the physical laws governing the evolution of a system with the information contained in the (partial and noised) observation of that system. From an inverse problem perspective, one may say that observations are analyzed using the prior information supplied by a

prognostic numerical model of the physics assumed to be at their origin. This inverse problem (cast in a time-dependent setting) can be tackled using either a sequential or a variational approach (consult *Talagrand* [1997] for a concise introduction to both).

[3] In the context of terrestrial magnetism, *Canet et al*. [2009] and *Li et al*. [2011] reported preliminary efforts on the variational front, and a first geophysical application of variational assimilation was performed by *Gillet et al*. [2010] in their study of torsional waves within Earth's core. Following a complementary strategy, the sequential approach was tested in depth by *Kuang et al*. [2008, 2009], using a three-dimensional, convection-driven model of the geodynamo as physical model of the secular variation. This led these authors to contribute to the latest generation of the International Geomagnetic Reference Field [*Finlay et al*., 2010], by means of a candidate secular variation model [*Kuang et al*., 2010].

[4] The difficulty in applying sequential assimilation schemes to the geodynamo arises from the conjunction of the size of the problem and of its nonlinearity. The latter is generally handled by means of some modified version of the Kalman filter, whose optimality is conditioned to the linearity (and Gaussianity) of the problem at hand. The former makes the propagation of the forecast error covariance out of practical reach. Consequently, the studies quoted above, in addition to the more recent work by *Aubert and Fournier* [2011], assumed frozen forecast error statistics, thereby resorting to a method mistakenly termed optimal interpolation.

[5] The goal of this technical note is to present the application of a more sophisticated sequential method, known as the ensemble Kalman filter (EnKF), to a three-dimensional dynamo model. We recall the basic principles of the EnKF and describe our implementation strategy in section 2. Section 3 presents the results of a series of closed-loop experiments used for validation. We summarize our findings and discuss directions for future work in section 4.

2. Principle and Implementation of the Ensemble Kalman Filter

[6] The EnKF [*Evensen*, 1994; *Burgers et al*., 1998] uses the traditional update equation of the Kalman Filter, save that the Kalman gain matrix is calculated from the error covariances provided by the ensemble of model states. Its relative ease of implementation and affordable computational requirements have made it a sequential data assimilation method of choice for nonlinear problems (see *Evensen* [2009], section B1 for a comprehensive overview of its various applications). The fundamentals of the EnKF are recalled in Table 1.

[7] We start from a numerical dynamo model, the Parody code [*Dormy et al*., 1998; *Aubert et al*., 2008]. The implementation of the EnKF layer is based on the parallel data assimilation framework (PDAF), described by *Nerger et al*. [2005] and *Nerger and Hiller* [2013], and applied by these authors to an oceanographic problem. PDAF is an a message passing interface (MPI)-based framework whose application upon a pre-existing parallel code is relatively straightforward, provided the starting code has a sufficiently modular structure [*Nerger and Hiller*, 2013, Figure 1]. To ease our implementation of PDAF, we, therefore, begun by increasing the modularity of the basic Parody code. What PDAF does in practice is to define its own set of MPI communicators in addition to the pre-existing set of communicators used by the dynamo model. The PDAF set essentially handles the ensemble (e.g., it feeds each ensemble member with an analyzed initial condition for subsequent forward integration, effectively linking equation (8) with equation (1) in Table 1; the interested reader is invited to consult the work by *Nerger and Hiller* [2013] for a complete description of the capabilities of PDAF).

[8] For each ensemble member, the state vector includes, at each radial level, the spherical harmonic coefficients of the poloidal and toroidal scalars used to represent the flow and the magnetic field, in addition to the spectral coefficients describing the codensity field. Since Parody relies on complex spherical harmonics, the state vector is a complex-valued vector field, a situation which is rather unusual and not implemented as such within the native PDAF package. We modified the core routines of PDAF accordingly; from an algebraic perspective, this essentially amounted to changing every transpose operation to a transpose-and-conjugation operation.

3. Validation Using Closed-Loop (Twin) Experiments

[9] In order to validate our implementation, we resort to closed-loop (also termed twin) experiments based on synthetic data. The specific

Table 1. Generic Description of the Ensemble Kalman Filter as Implemented in This Study[a]

1. Forecast

$$\mathbf{x}^f_{i,e} = M_{i-1,i}(\mathbf{x}^a_{i-1,e}), \quad e \in \{1, \ldots, N_e\}. \quad (1)$$

2. Analysis

$$\langle \mathbf{x}^f_i \rangle = \frac{1}{N_e} \sum_{e=1}^{N_e} \mathbf{x}^f_{i,e}, \text{ calculation of the mean } (2)$$

$$\mathbf{P}^f_i = \frac{1}{N_e - 1} \sum_{e=1}^{N_e} \left(\mathbf{x}^f_{i,e} - \langle \mathbf{x}^f_i \rangle \right) \left(\mathbf{x}^f_{i,e} - \langle \mathbf{x}^f_i \rangle \right)^\dagger \quad (3)$$

$$\mathbf{H}_i \mathbf{P}^f_i = \frac{1}{N_e - 1} \sum_{e=1}^{N_e} \left[H_i\left(\mathbf{x}^f_{i,e}\right) - H_i\left(\langle \mathbf{x}^f_i \rangle\right) \right] \left[\mathbf{x}^f_{i,e} - \langle \mathbf{x}^f_i \rangle \right]^\dagger \quad (4)$$

$$\mathbf{H}_i \mathbf{P}^f_i \mathbf{H}^\dagger_i = \frac{1}{N_e - 1} \sum_{e=1}^{N_e} \left[H_i\left(\mathbf{x}^f_{i,e}\right) - H_i\left(\langle \mathbf{x}^f_i \rangle\right) \right] \left[H_i\left(\mathbf{x}^f_{i,e}\right) - H_i\left(\langle \mathbf{x}^f_i \rangle\right) \right]^\dagger \quad (5)$$

$$\mathbf{K}_i = \left(\mathbf{H}_i \mathbf{P}^f_i \right)^\dagger \left[\mathbf{H}_i \mathbf{P}^f_i \mathbf{H}^\dagger_i + \mathbf{R}_i \right]^{-1}, \text{ calculation of the Kalman gain } (6)$$

$$\mathbf{y}^o_{i,e} = \mathbf{y}^o_i + \varepsilon^o_e, \quad e = \{1, \ldots, N_e\}, \quad (7)$$

$$\mathbf{x}^a_{i,e} = \mathbf{x}^f_{i,e} + \mathbf{K}_i \left[\mathbf{y}^o_{i,e} - H_i\left(\mathbf{x}^f_{i,e}\right) \right], \quad e \in \{1, \ldots, N_e\}. \text{ update } (8)$$

[a]An ensemble of N_e forecasts $\mathbf{x}^f_{i,e}$ is generated at discrete time t_i by forward integration of each ensemble member e using the nonlinear dynamo model M between discrete times t_{i-1} and t_i (we assume without loss of generality that the last analysis was carried out at time t_{i-1}). The ensemble allows us to estimate the first and second statistical moments of the probability density function of the model state $\mathbf{x}$, namely the mean $\langle \mathbf{x}^f_i \rangle$ and covariance matrix $\mathbf{P}^f_i$. We have at hand a set of observations $\mathbf{y}^o_i$, with error ε^o_i. The knowledge of the (possibly nonlinear) observation operator H_i and of the observation error covariance matrix $\mathbf{R}_i$ makes it possible to compute the Kalman gain matrix (equation (6)) and to correct each forecast (equation (8)) for subsequent integration by the model. Note in equation (7) that, following *Burgers et al*. [1998], the observation feeding each ensemble member is noised, assuming Gaussian statistics with covariance $\mathbf{R}_i$. In these equations, a dagger means transpose conjugation. Both $\mathbf{R}_i$ and $\mathbf{P}^f_i$ are Hermitian matrices.

dynamo model used in order to generate our synthetic data is described at length in the work of *Fournier et al*. [2011], where it served as the source of prior information for the estimation of core surface flow at epoch 2010.0. This is a model of intermediate resolution (90 radial levels with a horizontal harmonic truncation at degree and order 64). It is driven by chemical buoyancy, with prescribed codensity at the inner-core boundary and zero codensity flux at the core-mantle boundary. The four nondimensional control parameters are the Ekman number, the Prandtl number, the magnetic Prandtl number, and the flux-based modified Rayleigh number, whose values are set to 10^{-3}, 1,

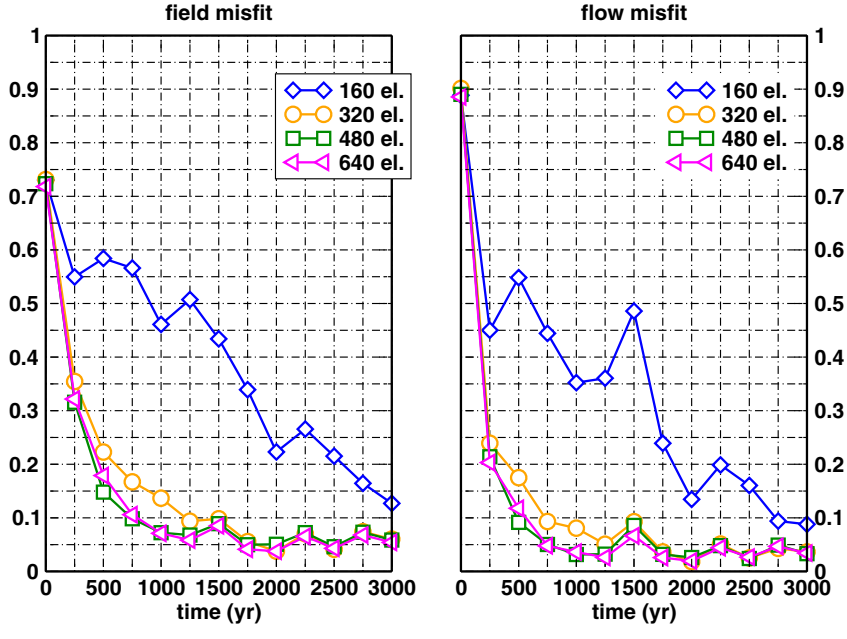

Figure 1. (left) Field and (right) flow energetic misfits as a function of time during closed-loop experiments for increasing ensemble sizes: 160 (diamonds), 320 (circles) 480 (squares), and 640 (triangles).

4, and $5.8\,10^{-4}$, respectively. The magnetic Reynolds number (an output of the simulation) has an average value of 100. This model is characterized by a moderate level of geophysical semblance, according to the static morphological criteria defined by *Christensen et al*. [2010]. Most notably, the high-latitude surface flux patches generated by the dynamo are too concentrated with respect to their geophysical counterparts. In addition, the model lacks equatorial features and their dynamics as revealed by the historical geomagnetic field model gufm1 [*Jackson et al*., 2000] (consult *Fournier et al*. [2011] for a detailed description of the model and its features).

[10] The state vector has a size close to 10^6 (965,250 precisely). The resolution used makes it possible to run ensemble calculations at an affordable computational cost. For example, our largest run, which comprised 640 members, took 12 h on 1440 cores (distributed over 45 IBM x3750-M4 nodes interconnected with a FDR10 Mellanox Infiniband network, visit http://www.idris.fr/eng/ada/hw-ada-eng.html for more details). The parallel efficiency (measured by the ratio of the total cpu time to the product "number of cores times execution time") was above 99%.

[11] The synthetic database is based on a free model run spanning several magnetic diffusion times. We extract from this reference dynamical trajectory a segment of duration 3500 years. We assume that observations are made every 25 years over the first 3000 years of this segment, and leave the ensemble unconstrained over the last 500 years, during which we will be able to estimate how long the ensemble can make a faithful prediction of the evolution of the system.

[12] A given observation is defined as a map of the radial component of magnetic induction, B_r, at the top of the core, truncated at spherical harmonic degree and order L and M, respectively (note that we will take $M = L$ throughout). Each truncated map is assimilated into the system in the form of a vector of complex-valued spectral coefficients (β_l^m, say) describing its spherical harmonic expansion. We will consider in the following two end-member situations, setting $L = 13$ (the best case scenario) or $L = 5$ (the worst case scenario). Data are noised, and, unless otherwise stated, we consider that the observational error covariance matrix $\mathbf{R}$ is diagonal and constant in time (we prescribed it based on the variances of the β_l^m during the first 500 years of the reference trajectory). This choice of $\mathbf{R}$ results in small scales of B_r being less well constrained than large scales (the relative accuracy decreases by one order of magnitude going from $l = 1$ to $l = 10$). In all cases, the observation error statistics used for our assimilation experiments match those imposed on the observations.

[13] In the tests reported below, we begin by studying the impact of the ensemble size on the quality of the estimate of the internal dynamo structure. This allows us to estimate a minimum size for the filter to behave properly. Based on this analysis, we next study how the quality of surface observations influences the quality of the recovery of the internal dynamo structure (in the best and worst case scenarios). We finally touch on the predictive power of the system, looking at the estimate of the axial dipole coefficient over the 3500 years of the experiment.

3.1. Ensemble Size

[14] The initial ensemble is formed by a collection of N_e snapshots taken randomly from the model free run, leaving aside the 3500 years defining the reference dynamical trajectory used for validation. Our estimate of the dynamo state vector, $\hat{\mathbf{x}}$, is provided by the ensemble mean

$$\hat{\mathbf{x}} \equiv \frac{1}{N_e}\sum_{e=1}^{N_e}\mathbf{x}_e. \tag{9}$$

[15] The knowledge of the reference dynamical trajectory makes it possible to measure the relative distance between the estimate and the truth. Following *Aubert and Fournier* [2011], we do so by computing the flow ($\mathbf{u}$) and magnetic field ($\mathbf{B}$) misfits, defined as

$$m_{\mathbf{u}} \equiv \frac{\int (\mathbf{u}^t - \hat{\mathbf{u}})^2 \mathrm{d}V}{\int (\mathbf{u}^t)^2 \mathrm{d}V} \tag{10}$$

and

$$m_{\mathbf{B}} \equiv \frac{\int (\mathbf{B}^t - \hat{\mathbf{B}})^2 \mathrm{d}V}{\int (\mathbf{B}^t)^2 \mathrm{d}V}, \tag{11}$$

respectively, and where we understand that the superscript t means "true" and that integrations are performed over the volume of the spherical shell.

[16] Figure 1 shows how this distance evolves as a function of time over the 3000 years during which data are available, for four different ensemble sizes, $N_e = 160$, 320, 480, and 640, assuming a good knowledge of the surface field (best case scenario, $L = 13$). In all instances, the distance decreases as a function of time, showing the positive impact of surface observations on the three-dimensional estimate of the state of the system. This is a positive consequence of the long-range correlations that exist between the surface poloidal magnetic field and the other state variables in the core interior, already reported by *Aubert and Fournier* [2011] in their optimal interpolation (OI) study of the same reference dynamo model. These correlations impact the analysis, since they are naturally included in the forecast error covariance matrix and subsequently in the Kalman gain matrix (Table 1). Comparison of Figure 4 (bottom) of *Aubert and Fournier* [2011] with Figure 1 highlights the superiority of the EnKF over OI, the former benefiting from the possibility of updating the forecast error covariance matrix as new data become available. Note as well that *Aubert and Fournier* [2011] found it useful to modify the OI formulation in order to reduce the attraction toward data (see the β factors in their analysis equation (17)), as they noticed otherwise, upon analysis, an overshoot of the estimated state with respect to the sought synthetic truth. The methodology used here does not require that type of empirical fix.

[17] The ensemble size affects the rate of convergence toward the true solution. If one has millennial-scale applications in mind based on a model of similar resolution, it appears that 480 ensemble members are required, since they allow for a faster spin-up of the system (inspection of Figure 1 indicates a spin-up time of about 1000 years). 320 members lead ultimately to the same estimate of the system, but only after about 2000 years. In the other experiments discussed below, we will, therefore, use 480 ensemble members to sample the probability density of dynamo states.

[18] Figure 1 shows that field and flow converge at the same rate. Note that we monitored independently the convergence of the toroidal and poloidal magnetic fields, in order to detect a possible difference which would reflect the fact that we only observe the large scales of the latter at the shell surface. We found very similar behaviors and conclude that convergence is uniform in state space.

3.2. Effect of the Resolution of Surface Observations on the Estimate

[19] Considering in the remainder of this study ensembles comprising 480 members, we now study the impact of the quality of surface observations (in the best and worst case scenarios) on the retrieval of the internal structure. Figure 2 shows maps of the radial component of magnetic induction and of the azimuthal component of flow, both at shell mid-depth, after 1000 years, that is the spin-up time of the system. Also shown are the maps of the difference between the reference and each estimate (multiplied by a factor of 5). Visual comparison of the second column from left (which has $L = 13$) with the leftmost column (the reference) confirms what could be anticipated from the previous analysis, namely that the mean of the ensemble provides a good estimate of the internal structure, under these admittedly favorable circumstances. Most of the prominent features are in place, with appropriate location and amplitude. This is particularly true for the convective cartridge belt of westward flow in the tropics. In the worst case scenario now ($L = 5$, third column from left), the estimate of the internal structure is less satisfactory, a consequence of the more modest information provided by the observations. Some of the structures are still in place though, in most instances with less detail and a lower amplitude. That being said, the mid-latitude flux patch at $(180E, 45N)$ is, for example, well estimated, as is the underlying flow structure. It is noteworthy that the local level of detail reached in some places is better than what could be anticipated from the $L = 5$ truncation of surface observations. This is a benefit of the nonlinear character of the dynamo, which makes it possible for information to cascade down the magnetic and kinetic spectra. In order to illustrate this point further, we show in the rightmost column of Figure 2 results obtained assimilating observations still truncated at $L = 5$, but considering this time the full observation error covariance matrix, in contrast to the diagonal assumption made so far. (Our prescription of off-diagonal covariances between the β_l^m is, as before, based on the statistics of the first 500 years of the reference trajectory.) When this substantial piece of extra information is supplied to the system, we get estimates of the internal structure of a quality as good as that obtained in the best case scenario. This is a very encouraging result, which stresses the need to resort to full covariance matrices when assimilating observations in the form of time-dependent Gauss coefficients describing the core surface field.

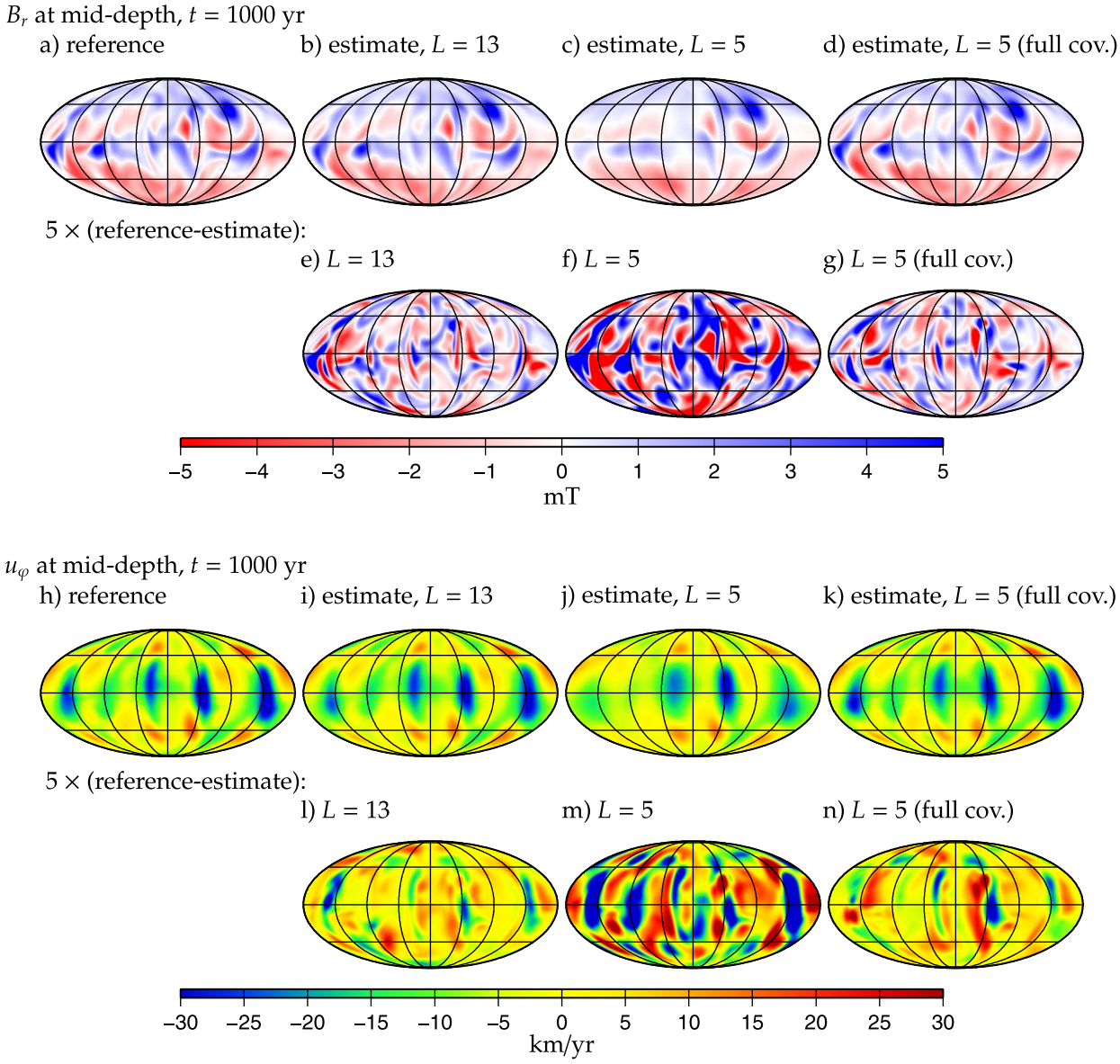

Figure 2. Estimate of the internal dynamo structure after 1000 years of assimilation of synthetic data. Top two rows: radial magnetic induction at midshell depth. Top row, from left to right: reference, estimates with data truncated at degree 13, 5, and 5 again, using that time a full observation error covariance matrix. Second row from top, from left to right: maps of the difference between the reference and the estimate (multiplied by a factor of 5), with data truncated at degree 13, 5, and 5, using a full observation error covariance matrix. Bottom two rows: same sequence for the azimuthal velocity at mid-depth. Mollweide projections.

3.3. Behavior of the Axial Dipole Coefficient

[20] Figure 3 shows the behavior of the axial dipole Gauss coefficient, g_1^0, over the 3500 years of the experiments, in the best and worst case scenarios. Both scenarios consider the same initial ensemble, which is biased toward values stronger than needed when compared with the reference (see the flat histograms labeled with a (1) in Figure 3). As the EnKF system is adaptive, however, both best case and worst case forecast estimates are in line with the reference after the 1000 years of spin-up (see the blue curves on the topmost and bottommost time series, respectively). The differences are to be found in the scatter of the ensemble about the mean, which is wider in the $L = 5$, less tightly constrained, situation. Accordingly, after the 3000 years of assimilation (histograms labeled with a (2)), the best case distribution is remarkably

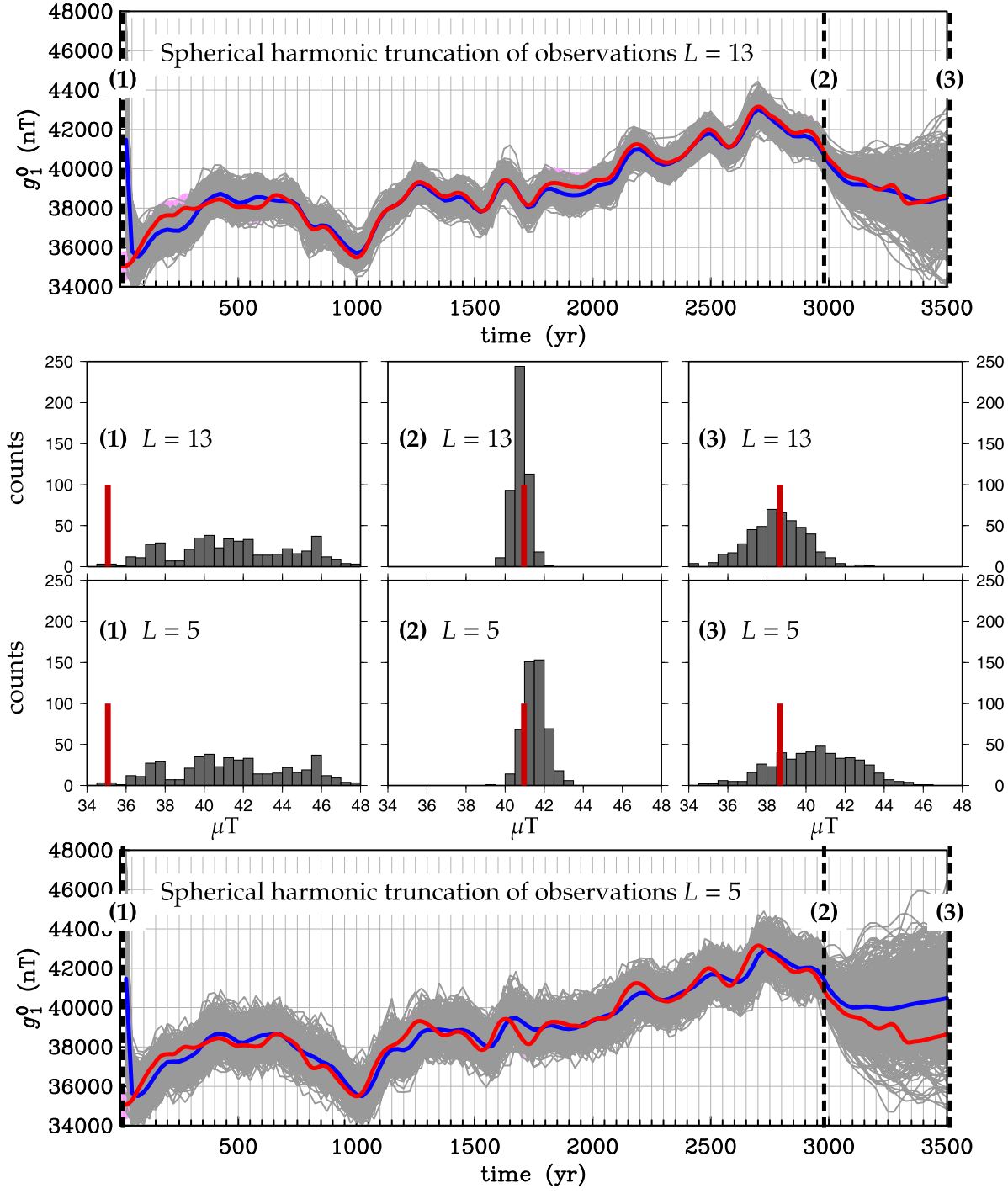

Figure 3. Behavior of the axial dipole Gauss coefficient g_1^0. Top two rows: $L = 13$ truncation of observations (using a diagonal error covariance matrix). Top row: time series of g_1^0 over the 3500 years of experiment. The red curve is the reference, with standard deviation indicated by the pink envelope. This envelope is most of the time covered with the ensemble of predictions for g_1^0 (one gray curve per member). The blue curve is the forecast estimate (the ensemble mean). Informations are supplied over the first 3000 years, after which the ensemble is no longer constrained. The vertical dashed lines labeled (1), (2), and (3) refer to $t = 0$ year, $t = 3000$ years, and $t = 3500$years , respectively. The corresponding distribution of forecasts are shown in the second row from top, with the truth shown in thick red for reference. The ensemble of g_1^0 are put into bins of width 500 nT. Bottom two rows: Same for a $L = 5$ truncation of observations (and a diagonal error covariance matrix). Bottom row: time series of g_1^0. Second row from bottom: histograms at $t = 0$ year, $t = 3000$ years, and $t = 3500$ years (from left to right).

peaked around the truth (central histogram, second row from top), whereas the $L = 5$ situation yields a broader distribution (central histogram, second row from bottom). It is also of interest to look at the evolution of the system for the remaining 500 years of experiment, when no more data are available. Inspection of the time series of the ensemble reveals that the scatter increases with time, a consequence of the chaotic character of the dynamo model, which causes the distance between two initially close trajectories to increase exponentially [*Hulot et al*., 2010; *Lhuillier et al*., 2011]. Figure 3 (top) shows that the scatter is approximately multiplied by a factor of 4 between $t = 3000$ years and $t = 3500$ years in the $L = 13$ case. This factor is consistent with the value of the *e*-folding time for this dynamo model, which is around 350 years [*Fournier et al*., 2011]. Despite this increase of the scatter (compare histograms labeled (3) and (2) in the second row from the top in Figure 3), the estimate is still in agreement with the reference, as it follows the long-term decrease of g_1^0. We ascribe this positive result to the quality of the estimate of the internal structure of the dynamo discussed in the previous section. When the internal structure is less well constrained ($L = 5$ scenario), the capability of the system to forecast the evolution of the axial dipole is hampered. Figure 3 (bottom) highlights the failure of the forecast to correctly predict the centennial-scale decrease in g_1^0. As an important aside, let us stress that if we use a full observation error covariance matrix in place of a diagonal one (recall Figure 2), the quality of the forecast of the evolution of g_1^0 in the $L = 5$ case is comparable to the one obtained in the $L = 13$ case.

4. Summary and Outlook

[21] We have presented and validated the application of the ensemble Kalman filter to a three-dimensional, convection-driven model of the geodynamo. Our synthetic experiments were based on observations consisting of spectral coefficients describing the poloidal magnetic field at the core surface, with truncation degree L set to 13 or 5.

[22] These experiments indicate that an ensemble size of $O(500)$ is in order for the EnKF to behave properly, with a spin-up time of the order of 1000 years. We find promising forecasting capabilities (as measured by the evolution of the axial dipole Gauss coefficient) in the $L = 13$ case. The $L = 5$ situation does not yield such satisfactory results, unless one resorts to a full observation error covariance matrix (as opposed to a diagonal one).

[23] This last point is particularly important for immediate geophysical applications of this method. We may begin by assimilating time-dependent parameterized models of the geomagnetic field as observations, considering initially models covering the past few millennia to centuries [e.g., *Korte et al*., 2011; *Korte and Constable*, 2011; *Licht et al*., 2013; *Jackson et al*., 2000; *Gillet et al*., 2013]. In this respect, we note with satisfaction that recent models now provide either the covariance matrix of Gauss coefficients directly [*Gillet et al*., 2013], or an ensemble of models [*Licht et al*., 2013], which makes the calculation of the covariance matrix straightforward.

[24] This process will allow us to exercise different models of the geodynamo, in a realistic situation where observations will not be necessarily compatible with the physics represented by the numerical model. As illustrated by the wedge in *Christensen et al*. [2010, Figure 7], and exemplified by the recent work of *Aubert et al*. [2013], this quest for dynamical Earth likeness will most probably require an increase of resolution, in comparison with the intermediate resolution used in this study.

Acknowledgments

[25] A.F. thanks Jeff Anderson and Geir Evensen for sharing their expertise. This work was supported by the French Agence Nationale de la Recherche under the grant ANR-2011-BS56-011. Numerical computations were performed at S-CAPAD, IPGP, France and using HPC resources from GENCI-IDRIS (grant 2013–042122). Figures were generated using the generic mapping tools of *Wessel and Smith* [1991], the plotxy software of Bob Parker (http://igppweb.ucsd.edu/~parker/Software/), and the pstricks-add LaTeX package (http://www.ctan.org/pkg/pstricks-add). This is IPGP contribution 3418.

References

Aubert, J., and A. Fournier (2011), Inferring internal properties of Earth's core dynamics and their evolution from surface observations and a numerical geodynamo model, *Nonlinear Processes Geophys.*, *18*, 657–674, doi:10.5194/NPG-18-657-2011.

Aubert, J., J. Aurnou, and J. Wicht (2008), The magnetic structure of convection-driven numerical dynamos, *Geophys. J. Int.*, *172*(3), 945–956.

Aubert, J., C. C. Finlay, and A. Fournier (2013), Bottom-up control of geomagnetic secular variation by the Earth's inner core, *Nature*, in press, DOI: 10.1038/nature12574.

Burgers, G., P. J. van Leeuwen, and G. Evensen (1998), Analysis scheme in the ensemble Kalman filter, *Mon. Weather Rev.*, *126*(6), 1719–1724.

Canet, E., A. Fournier, and D. Jault (2009), Forward and adjoint quasi-geostrophic models of the geomagnetic secular variation, *J. Geophys. Res.*, *114*, B11101, doi:10.1029/2008JB006189.

Christensen, U. R., J. Aubert, and G. Hulot (2010), Conditions for Earth-like geodynamo models, *Earth Planet. Sci. Lett.*, *296*(3–4), 487–496, doi:10.1016/j.epsl.2010.06.009.

Dormy, E., P. Cardin, and D. Jault (1998), MHD flow in a slightly differentially rotating spherical shell, with conducting inner core, in a dipolar magnetic field, *Earth Planet. Sci. Lett.*, *160*(1–2), 15–30.

Evensen, G. (1994), Sequential data assimilation with a nonlinear quasi-geostrophic model using Monte Carlo methods to forecast error statistics, *J. Geophys. Res.*, *99*, 10,143–10,162, doi:10.1029/94JC00572.

Evensen, G. (2009), *Data Assimilation: The Ensemble Kalman Filter*, 2nd ed., *307* p., Springer, Berlin, doi:10.1007/978-3-642–03711-5.

Finlay, C. C., et al. (2010), International geomagnetic reference field: The eleventh generation, *Geophys. J. Int.*, *183*(3), 1216–1230.

Fournier, A., G. Hulot, D. Jault, W. Kuang, A. Tangborn, N. Gillet, E. Canet, J. Aubert, and F. Lhuillier (2010), An introduction to data assimilation and predictability in geomagnetism, *Space Sci. Rev.*, *155*(1–4), 247–291, doi:10.1007/s11214-010-9669-4.

Fournier, A., J. Aubert, and E. Thébault (2011), Inference on core surface flow from observations and 3-D dynamo modelling, *Geophys. J. Int.*, *186*(1), 118–136, doi:10.1111/j.1365-246X.2011.05037.x.

Gillet, N., D. Jault, E. Canet, and A. Fournier (2010), Fast torsional waves and strong magnetic field within the Earth's core, *Nature*, *465*, 74–77, doi:10.1038/nature09010.

Gillet, N., D. Jault, C. C. Finlay, and N. Olsen (2013), Stochastic modelling of the Earth's magnetic field: Inversion for covariances over the observatory era, *Geochem. Geophys. Geosyst.*, *14*, 766–786, doi:10.1002/ggge.20041.

Hulot, G., F. Lhuillier, and J. Aubert (2010), Earth's dynamo limit of predictability, *Geophys. Res. Lett.*, *37*, L06305, doi:10.1029/2009GL041869.

Jackson, A., A. R. T. Jonkers, and M. R. Walker (2000), Four centuries of geomagnetic secular variation from historical records, *Philos. Trans. R. Soc. London A*, *358*(1768), 957–990.

Korte, M., and C. Constable (2011), Improving geomagnetic field reconstructions for 0–3 ka, *Phys. Earth Planet. Inter.*, *188*(3–4), 247–259, doi:10.1016/j.pepi.2011.06.017.

Korte, M., C. Constable, F. Donadini, and R. Holme (2011), Reconstructing the Holocene geomagnetic field, *Earth Planet. Sci. Lett.*, *312*(3–4), 497–505, doi:10.1016/j.epsl.2011.10.031.

Kuang, W., and A. Tangborn (2011), *Interpretation of core field models, in Geomagnetic Observations and Models, IAGA Special Sopron Book Series, vol. 5*, edited by M. Mandea and M. Korte, pp. 295–309, Springer, Netherlands, doi:10.1007/978-90-481-9858-0_12.

Kuang, W., A. Tangborn, W. Jiang, D. Liu, Z. Sun, J. Bloxham, and Z. Wei (2008), MoSST-DAS: The first generation geomagnetic data assimilation framework, *Commun. Comput. Phys.*, *3*, 85–108.

Kuang, W., A. Tangborn, Z. Wei, and T. Sabaka (2009), Constraining a numerical geodynamo model with 100-years of geomagnetic observations, *Geophys. J. Int.*, *179*(3), 1458–1468, doi:10.1111/j.1365-246X.2009.04376.x.

Kuang, W., Z. Wei, R. Holme, and A. Tangborn (2010), Prediction of geomagnetic field with data assimilation: A candidate secular variation model for IGRF-11, *Earth Planets Space*, *62*, 775–785.

Lhuillier, F., J. Aubert, and G. Hulot (2011), Earth's dynamo limit of predictability controlled by magnetic dissipation, *Geophys. J. Int.*, *186*, 492–508.

Li, K., A. Jackson, and P. W. Livermore (2011), Variational data assimilation for the initial-value dynamo problem, *Phys. Rev. E*, *84*(5, Part 2), 056,321, doi:10.1103/PhysRevE.84.056321.

Licht, A., G. Hulot, Y. Gallet, and E. Thébault (2013), Ensembles of low degree archeomagnetic field models for the past three millennia, *Phys. Earth Planet. Inter.*, in press, DOI: 10.1016/j.pepi.2013.08.007.

Nerger, L., and W. Hiller (2013), Software for ensemble-based data assimilation systems—Implementation strategies and scalability, *Comput. Geosci.*, *55*, 110–118, doi:10.1016/j.cageo.2012.03.026.

Nerger, L., W. Hiller, and J. Schröter (2005), A comparison of error subspace Kalman filters, *Tellus, Ser. A*, *57*(5), 715–735.

Talagrand, O. (1997), Assimilation of observations, an introduction, *J. Meteorol. Soc. Jpn.*, *75*(1B), 191–209.

Wessel, P., and W. H. F. Smith (1991), Free software helps map and display data, *Eos Trans. AGU*, *72*, 441–445, doi:10.1029/90EO00319.